Supplementary Information (SI) for Journal of Materials Chemistry A.
This journal is © The Royal Society of Chemistry 2025

Supporting Information

Probing the Mechanistic Role of Catalyst Layer Microstructure in Proton Exchange Membrane Water Electrolyzers

Navneet Goswami[ǂ], Abhinand Ayyaswamy[ǂ], Anindya Nath, Bairav S. Vishnugopi, and Partha P. Mukherjee[*]

School of Mechanical Engineering, Purdue University, West Lafayette, IN 47907, United States

*Correspondence: pmukherjee@purdue.edu

[ǂ] Equal contribution

S1. Description of microstructure aware PEMWE framework

In a typical Proton Exchange Membrane Water Electrolyzer (PEMWEs) cell (as shown in Fig. 1 of manuscript), the oxygen evolution reaction (OER) and hydrogen evolution reaction (HER) occur on the anode and the cathode side respectively that are driven by an electric potential to generate gaseous oxygen and hydrogen thereby making it a bubbly electrochemical system. Iridium (Ir) and carbon-supported Platinum (Pt) nanoparticles serve as catalytic materials respectively for the OER and HER. The proton-exchange membrane (PEM) that facilitates the passage of protons comprises perfluoro sulfonic acids (PFSA) which further act as the proton conducting material in the anode and cathode catalyst layer (ACL and CCL). The membrane electrode assembly (MEA) is compressed between a fibrous porous transport layer (PTL) on both sides of the anodic and cathodic compartments to facilitate the ingress of water and egress of the gaseous products. The system is sandwiched between two bipolar plates that act as the flow fields for the incoming feeds.

In PEM electrolysis, the overall water-splitting reaction is expressed as:

$$H_2O \rightarrow H_2 + {}^{1}\!/_{2}\, O_2 \tag{1}$$

Half-cell reaction at the anode side (oxygen evolution reaction):

$$H_2O \rightarrow {}^{1}\!/_{2}\, O_2 + 2H^+ + 2e^- \tag{2}$$

Half-cell reaction at the cathode side (hydrogen evolution reaction):

$$2H^+ + 2e^- \rightarrow H_2 \tag{3}$$

The mesoscale model is built on the conservation laws for species and charge transport under a single-phase approximation. The continuum modeling approach is employed to numerically solve the pertinent concentration and potential fields throughout the cell sandwich of the electrolyzer. The species balance equations are primarily assumed to be dominated by diffusive transport with the influence of bubble dynamics being accounted for through an auxiliary set of equations. The coupled set of equations solves for intrinsic variables which include the species $\left(c_{\mathrm{O}_2}, c_{\mathrm{H}_2}, c_{\mathrm{H_2O}}\right)$, solid, and electrolyte potentials (ϕ_s, ϕ_e) that directly impact the key macroscale observables in terms of power consumption and hydrogen throughput.

Conservation of charge: The charge conservation in solid-phase and electrolyte (ionomer) phase are described below:

$$\frac{\partial}{\partial x}\left(\sigma^{eff}\frac{\partial}{\partial x}\phi_s\right) - j = 0 \tag{4}$$

$$\frac{\partial}{\partial x}\left(\kappa^{eff}\frac{\partial}{\partial x}\phi_e\right) + j = 0 \tag{5}$$

In the above two equations, σ and κ denote the bulk electronic and ionic conductivity of the solid and ionomer phases respectively. For the membrane, the local charge conservation (Eq. 5) gets reduced to Ohm's law since the reaction source term, j is absent. It is important to note here that the ionic conductivity of the membrane and both the catalyst layers is a strong function of the water content and operating temperature.

For a PEMWE system that displays sluggish oxygen evolution reaction (OER) at the anode, the electrochemical reaction current described by the Butler-Volmer equation can be recast into a positive half of the Tafel equation:

$$j_a = j_{OER} = a_a i_{0,OER} \exp\left(\frac{\alpha_a F}{RT}\eta\right) \tag{6}$$

On the other hand, hydrogen evolution reaction kinetics (HER) at the cathode is represented by the negative half of the Tafel equation, as expressed below:

$$j_c = j_{HER} = -a_c i_{0,HER}\left(\frac{c_{\mathrm{H}^+}}{c_{\mathrm{H}^+,\mathrm{ref}}}\right)\exp\left(-\frac{\alpha_c F}{RT}\eta\right) \tag{7}$$

Here, a is the specific active surface area or the roughness factor of the catalyst layers, which in turn is a product of the electrochemical active area (ECA) and the catalyst loading, $i_{0,OER}$ and $i_{0,HER}$ are the pertinent exchange current densities, α_a and α_c are the anodic and cathodic transfer coefficients for the corresponding electrochemical reaction. Also, the subscripts a and c indicate the anode and cathode respectively. Overpotential η refers to the differential between the solid phase potential, electrolyte phase potential, and the open circuit potential (OCP) for each electrode which can be given by the following expression[1,2]:

$$\eta = \phi_s - \phi_e - \left(U\left(p,T\right) - \frac{2.303RT}{F}pH\right) \tag{8}$$

Conservation of species: The mass transport mechanisms in the porous transport layer and the catalyst layers are essentially governed by diffusion phenomena. For the mathematical treatment of the diffusion of dissolved gases, we employ Fick's law of diffusion. The mass balance equation is defined in terms of molar concentration which yields,

$$\frac{\partial}{\partial x}\left(D_i^{eff}\frac{\partial}{\partial x}C_i\right) + S_i = 0 \tag{9}$$

In the above equation, C_i represents the concentration of species *i* in the gaseous phase and D_i is its diffusivity. To denote the effective diffusivity of the porous media, we use the subscript *eff*. Based on Faraday's law, the reaction term in Eq. 9, S_i can be expressed as $-\frac{s_i j}{nF}$ for a generic electrochemical reaction being designated as $\sum_i s_i M_i^z = n_e e^-$, where, M_i is the chemical formula of species *i*, n_e is the number of electrons exchanged and s_i is the stoichiometric coefficient. It is important to note that S_i reduces to zero for both the PTLs and the ion-conducting membrane. The species conservation equation for the relevant participating species and the reaction terms are mentioned below.

Species conservation equation for O_2:

$$\frac{\partial}{\partial x}\left(D_{\mathbf{O_2}}^{eff}\frac{\partial}{\partial x}C_{\mathbf{O_2}}\right)+S_{\mathbf{O_2}}=0 \tag{10}$$

Source term for O_2 species:

$$\begin{aligned} &\text{ACL:} && S_{\mathrm{O_2},a}=\frac{j_a}{4F} \\ &\text{CCL:} && S_{\mathrm{O_2},c}=0 \end{aligned} \tag{11}$$

Species conservation equation for H_2:

$$\frac{\partial}{\partial x}\left(D_{\mathbf{H_2}}^{eff}\frac{\partial}{\partial x}C_{\mathbf{H_2}}\right)+S_{\mathbf{H_2}}=0 \tag{12}$$

Source term for H_2 species:

$$\begin{aligned} &\text{ACL:} && S_{\mathrm{H_2},a}=0 \\ &\text{CCL:} && S_{\mathrm{H_2},c}=\frac{-j_c}{2F} \end{aligned} \tag{13}$$

Species conservation equation for H_2O:

$$\frac{\partial}{\partial x}\left(D_{\mathbf{H_2O}}^{eff}\frac{\partial}{\partial x}C_{\mathbf{H_2O}}\right)+S_{\mathbf{H_2O}}=0 \tag{14}$$

Source term for H_2O species:

$$\begin{aligned} &\text{ACL:} && S_{\mathrm{H_2O},a}=\frac{-j_a}{2F} \\ &\text{CCL:} && S_{\mathrm{H_2O},c}=0 \end{aligned} \tag{15}$$

The water molecules are transported via the protonic current to the cathode side through the mechanism of electroosmotic drag. This phenomenon is present only where ionic current exists, i.e., in the catalyst layers and membrane, and is trivial for other transported species in the PEMWE like H_2 and O_2. The pertinent boundary conditions are listed in Table S1 of the Supporting Information.

S2. Incorporating bubble coverage and dynamics to PEMWE framework

At low current densities, the mass transport limitation is purely diffusion limited. However, at large current densities, when the gas production rises, the electrolysis reaches a supersaturation stage, such that the bubble population increases manifold. The production of bubbles leads to the buildup of local resistances through the coverage of catalytic sites that contribute to the electrochemical reactions. The estimation of bubble coverage and its implications on the passivation of active areas are discussed below. Fig. S1 shows the schematic of a bubble-electrode interaction that governs the overall reaction kinetics at the catalyst surface. Based on the bubble size and contact angle on the substrate, the volume of the bubble before detachment can be quantified as follows[3,4]:

$$V_b = \frac{\pi r_b^3}{3}\left(2 + 3\cos\theta - \cos^3\theta\right) \tag{16}$$

where, r_b is the radius of the bubble and θ is the static contact angle.

The ideal gas relation can be rewritten in terms of the bubble volume based on the expression from Eq. 17:

$$p\frac{\pi r_b^3}{3}\left(2 + 3\cos\theta - \cos^3\theta\right) = nRT \tag{17}$$

Based on Faraday's law, the rate of gas generation is written below:

$$\dot{n} = \frac{IA}{n_e F} \tag{18}$$

where, I is the operating current density (units of A/m^2).

The rate of gas generation is related to the number of moles produced through the expression:

$$n = \dot{n}t \tag{19}$$

The generation rate for a single bubble takes the form[4]:

$$n' = \frac{\dot{n}}{n_b} \tag{20}$$

where, n_b is the total number of bubbles. Using Eqs. 17-20, the radius for one bubble can be found as:

$$r_b = \left[\frac{3\left(\frac{IA}{n_e F n_b} \right) RT}{\pi p \left(2 + 3\cos\theta - \cos^3\theta \right)} t \right]^{1/3} \tag{21}$$

Based on the bubble radius, the bubble coverage or the fraction of electrode surface shielded by the electrogenerated bubbles can be expressed as[5]:

$$\Theta = \frac{n_b}{At} \int_0^{t_{res}} \pi \sin^2\theta r_b^2 dt \tag{22}$$

Plugging the expression for bubble radius from Eq. 21 into Eq. 22 yields:

$$\Theta = \frac{3}{5} \pi \sin^2\theta \left(\frac{n_b}{A} \right) \left[\frac{3IART}{\pi p n_e F n_b \left(2 + 3\cos\theta - \cos^3\theta \right)} \right]^{2/3} t_{res}^{2/3} \tag{23}$$

Once the information on the bubble coverage is known, the unshielded active area can be corrected in terms of an effective area, which takes the following form:

$$a_{eff} = a\left(1 - \Theta\right) \tag{24}$$

S3. Quantification of overpotential and resistive modes

To minimize power consumption, lower cell voltages are desirable for a given current density for the same amount of hydrogen production, meaning a higher stack efficiency. The voltage drawn by the PEMWE takes into account the reversible potential and the contribution from three overpotential modes namely, activation overpotential (occurring at the interface of the electrode and electrolyte); ohmic overpotential (owing to the membrane resistance), and mass transport or concentration overpotential (owing to the bubble evolution at the anode and cathode and slow diffusion of the evolved gases):

$$V = E^{OCV} + |\eta|_{kinetic}^{anode} + |\eta|_{kinetic}^{cathode} + |\eta|_{ionic,total} + |\eta|_{electronic,total} + |\eta|_{mt,total} \tag{25}$$

The kinetic overpotential considers the effect of activation resistances from both the anode and cathode. However, if the cathode employs the standard Pt/C catalyst, the HER exhibits facile kinetics such that the cell activation overpotential is mostly dictated by the slow OER on the anode side.

$$|\eta|_{kinetic}^{anode} = \frac{1}{L_{ACL}} \int \eta dx, \text{ where, } \eta = \phi_s - \phi_e - \left(U^{OER}\left(p,T\right) - \frac{2.303RT}{F} p\mathrm{H} \right) \tag{26}$$

$$|\eta|_{kinetic}^{cathode} = \frac{1}{L_{CCL}} \int \eta dx, \text{ where, } \eta = \phi_s - \phi_e - \left(U^{HER}\left(p,T\right) - \frac{2.303RT}{F} p\mathrm{H} \right) \tag{27}$$

The ohmic overpotential originates from (i) the ionic resistance of the membrane and the catalyst layers which is dependent on the hydration state of the electrolyzer, and (ii) the electrical resistance of catalyst layers, porous transport layers, and bipolar plates.

In the mass-transport controlled regime, the rate of the water splitting reaction is dictated by the mass balance of the rate of reactant water supply and the efflux of the produced gaseous streams from the electrode. Of particular importance is the gas-evolving electrode at the anode side. At high current densities, the evolution of oxygen bubbles passivates the reactant sites and hampers the catalyst utilization by reducing the electrochemical active area in addition to altering the pH and thermal microenvironment. The dynamics of the electrogenerated bubbles and the slow diffusion of gases pose mass transport limitations which together constitute the concentration overpotential. In that case, the slow removal of the dissolved gases in the electrochemical reactors can be estimated through a Nernst equation similar to that used in fuel cells[6,7]:

$$\eta_{diffusion,anode} = \left(\frac{RT}{n_e F}\right)\ln\left(\frac{c_{\mathrm{O_2}}}{c_{\mathrm{O_{2,ref}}}}\right) \tag{28}$$

$$\eta_{diffusion,cathode} = \left(\frac{RT}{n_e F}\right)\ln\left(\frac{c_{\mathrm{H_2}}}{c_{\mathrm{H_{2,ref}}}}\right) \tag{29}$$

Since the mass transport limitation is more significant on the anode side, where the water splitting reaction takes place, the bubble overpotential at the anode can be expressed as:

$$\eta_{bubble,anode} = \left(\frac{RT}{n_e F}\right)\ln\left(\frac{1}{1-\Theta}\right) \tag{30}$$

Finally, the total mass transport overpotential can be expressed as:

$$\eta_{mt.total} = \eta_{diffusion,anode} + \eta_{diffusion,cathode} + \eta_{bubble,anode} \tag{31}$$

To derive detailed insights regarding the individual contribution of each mechanism, we translate the overpotentials introduced in the previous section into resistances which are mathematically expressed below:

Kinetic resistance at the anode:

$$R_{kinetic,anode} = \frac{\eta_{kinetic,anode}}{I} \tag{32}$$

Kinetic resistance at the cathode:

$$R_{kinetic,cathode} = \frac{\eta_{kinetic,cathode}}{I} \tag{33}$$

Ionic resistance:

$$R_{ionic} = \frac{\eta_{ionic,ACL} + \eta_{ionic,PEM} + \eta_{ionic,CCL}}{I} \tag{34}$$

Electronic resistance:

$$R_{electronic} = \frac{\eta_{electronic,APTL} + \eta_{electronic,ACL} + \eta_{electronic,CCL} + \eta_{electronic,CPTL}}{I} \tag{35}$$

Mass-transport resistance:

$$R_{mt} = \frac{\eta_{diffusion,ACL} + \eta_{diffusion,CCL} + \eta_{bubble,ACL}}{I} \tag{36}$$

S4. Description and evaluation of microstructural attributes

The electrodes have three definite phases- catalyst/support, ionomer and pore spaces and will be designated henceforth as phase 1, 2 and 0 respectively. The microstructure backbone was realized using a commercial tool GeoDict[8], which has the capability to use a stochastic reconstruction algorithm to generate synthetic phase 1 base for addition of phase 2. The various relations used for calculations of the volume fractions of phase 1 and phase 2 for the ACL and CCL are delineated below: -

$$\varepsilon_{catalyst,ACL} = \frac{\rho_{ACL}}{D_{catalyst} L_{ACL}} \tag{38}$$

$$\varepsilon_{ionomer,ACL} = \frac{w_{ionomer}}{D_{ionomer}\left(1 - w_{ionomer}\right)} \frac{\rho_{ACL}}{L_{ACL}} \tag{39}$$

$$\varepsilon_{ionomer,CCL} = \frac{R_{C/Pt} R_{ionomer/C}}{D_{ionomer}} \frac{\rho_{Pt}}{L_{CCL}} \tag{40}$$

$$\varepsilon_{CCL} = 1 - \left[\frac{1}{D_{Pt}} + \frac{R_{C/Pt}}{D_C} + \frac{R_{C/Pt} R_{ionomer/C}}{D_{ionomer}} \right] \frac{\rho_{Pt}}{L_{CCL}} \tag{41}$$

Where ρ, D, w, and L stands for catalyst loading, density, weight fraction and thickness respectively.

The electrochemical active area $\left(a_s\right)$ tortuosity $\left(\tau\right)$ and the effective transport properties *viz.* effective ionic conductivity $\left(\kappa^{eff}\right)$ and the effective electronic conductivity $\left(\sigma^{eff}\right)$ were estimated using direct numerical simulation (DNS) on the reconstructed microstructures. The electrochemical active area has been calculated using a modified form of the Minkowski method[9] as follows-

$$a_s = \frac{4\pi I_{1-2}}{M_x M_y M_z \Delta} f \tag{42}$$

Where M_x, M_y and M_z are the number of voxels in x, y and z direction respectively, I_{1-2} is the number of faces with phase 1 and phase 2 on either side and Δ is the voxel length. The factor *f* is computed because of the convergence of a digitized sphere having radius $\left(r = N\Delta\right)$ and number of faces (=I_N) given by, $f = \dfrac{N^2}{I_N}$. When the number of faces is large enough, the sphere approaches the shape of an ideal sphere with surface area $4\pi r^2$.

The calculation of the tortuosity in phase 2 is performed by solution of the Laplace equation $\left(\nabla^2 c = 0\right)$ on the reconstructed microstructure, where *c* is the concentration. For the estimation of tortuosity τ_x in x- direction, the imposed boundary conditions are- $c(x=0)=0$, $c(x=L_x)=1$ and $\mathbf{n}\cdot\nabla c = 0$ for the other faces. The flux, J_x is then computed by integrating the concentration gradient, $\partial c / \partial x$ over one of the extreme faces. For this calculation, the diffusivity in the solid electrolyte phase is 1 and those in the pore and active material phases are taken as 0. Finally, the x-direction tortuosity, τ_x is calculated using-

$$J_x = -\frac{\varepsilon_2}{\tau_x}\left(\frac{c|_{x=L_x} - c|_{x=0}}{L_x}\right) \tag{43}$$

Where, ε_2 is the volume fraction of phase 2. Similarly, τ_y and τ_z are calculated and finally, the mean tortuosity in the solid electrolyte is given by-

$$\tau = \frac{\tau_x + \tau_y + \tau_z}{3} \tag{44}$$

The effective ionic conductivity is then calculated by-

$$\kappa^{eff} = \kappa^{bulk}\frac{\varepsilon_2}{\tau} \tag{45}$$

Where, κ^{bulk} is the bulk intrinsic conductivity of phase 2, which is a material property.

The effective electronic conductivity estimation is conducted in a similar fashion, by the solution of the Laplace's equation for electric potential in phase 1 $\left(\nabla\cdot\left(\sigma\nabla\phi\right)=0\right)$; where σ is the dimensionless electronic conductivity which is assigned values 1 in phase 1 and 0 in the pore and phase 2 respectively. For the estimation of dimensionless electronic conductivity, σ_x in x-direction, the imposed boundary conditions are- $\phi(x=0)=0$, $\phi(x=L_x)=1$ and $\mathbf{n}\cdot\nabla\phi=0$ for the other faces. The effective electronic conductivity, σ_x in x- direction is calculated as follows-

$$\sigma_x = \left(\int_{y-z,plane} \sigma \left.\frac{\partial \phi}{\partial x}\right|_{x=0} dydz \right) \Bigg/ \left(\frac{\left.\phi\right|_{x=L_x} - \left.\phi\right|_{x=0}}{L_x} \right) \tag{46}$$

Similarly, σ_y and σ_z are calculated. The mean dimensionless electronic conductivity is given by-

$$\sigma = \frac{\sigma_x + \sigma_y + \sigma_z}{3} \tag{47}$$

The effective electronic conductivity of phase 1 is then given by-

$$\sigma^{eff} = \sigma^{bulk}\sigma \tag{48}$$

Where, σ^{bulk} is the bulk intrinsic conductivity of phase 1.

To ensure that the estimation of effective transport properties is independent of the choice of domain size, the entire protocol beginning with generation of microstructure till estimation of effective transport properties is repeated for multiple lengths (*L*), and voxel lengths (Δ). The optimum value is estimated to be *L*=16*R* and Δ=*R*/16, where *R* is the radius of the catalyst particles in the catalyst layers.

S5. Evaluation of performance metrics in PEMWE

The specific energy consumption (SEC) of PEMWE is a key performance metric which quantifies and reflects the efficiency of the electrolyzer stack. It is defined as the electrical power (in kW) required to produced one kilogram of hydrogen in one second and can be mathematically expressed as: -

$$SEC = \frac{n_{stacks} \times operating\ power\ consumption\ \left(kW\right)}{3600 \times operating\ mass\ flow\ rate,\ or\ hydrogen\ throughput\ \left(kg/s\right)} \tag{49}$$

The SEC is representative of the overall efficacy of the electrolyzer as it is dependent on the operating current density, the cell voltage, and the hydrogen throughput which in turn is dependent on the pore-scale electrochemical kinetics-flow-transport interactions. Lowering the SEC is one of the key focus areas in PEM electrolyzer technology development as it profoundly impacts the operational cost and the associated carbon footprint to produce hydrogen.

Table S1. Boundary conditions of state variables in the PEMWE framework

State variables	**BP-APTL interface** $(\boldsymbol{x=0})$	**APTL-ACL interface** $(\boldsymbol{x=L_{APTL}})$	**ACL-PEM interface** $(\boldsymbol{x=L_{APTL}+L_{ACL}})$	**PEM-CCL interface** $(\boldsymbol{x=L_{APTL}+L_{ACL}+L_{PEM}})$	**CCL-CPTL interface** $(\boldsymbol{x=L_{APTL}+L_{ACL}+L_{PEM}+L_{CCL}})$	**CPTL-BP interface** $(\boldsymbol{x=L_{APTL}+L_{ACL}+L_{PEM}+L_{CCL}+L_{CPTL}})$
ϕ_e	$\left.\frac{\partial \phi_e}{\partial x}\right\vert_x = 0$	$\left.\frac{\partial \phi_e}{\partial x}\right\vert_x = 0$	$\kappa^{eff}\nabla\phi_e\vert_{x-\delta} = \kappa^{eff}\nabla\phi_e\vert_{x+\delta}$	$\kappa^{eff}\nabla\phi_e\vert_{x-\delta} = \kappa^{eff}\nabla\phi_e\vert_{x+\delta}$	$\left.\frac{\partial \phi_e}{\partial x}\right\vert_x = 0;\ \phi_e = 0$	$\left.\frac{\partial \phi_e}{\partial x}\right\vert_x = 0$
ϕ_s	$\sigma_s^{eff}\left.\frac{\partial \phi_s}{\partial x}\right\vert_x = -I$	$\left.\left(\sigma_s^{eff}\frac{\partial \phi_s}{\partial x}\right)\right\vert_{x-\delta} = \left.\left(\sigma_s^{eff}\frac{\partial \phi_s}{\partial x}\right)\right\vert_{x+\delta}$	$\left.\frac{\partial \phi_s}{\partial x}\right\vert_x = 0$	$\left.\frac{\partial \phi_s}{\partial x}\right\vert_x = 0$	$\left.\left(\sigma_s^{eff}\frac{\partial \phi_s}{\partial x}\right)\right\vert_{x-\delta} = \left.\left(\sigma_s^{eff}\frac{\partial \phi_s}{\partial x}\right)\right\vert_{x+\delta}$	$\sigma_s^{eff}\left.\frac{\partial \phi_s}{\partial x}\right\vert_x = -I$
C_{O_2}	$\chi_{O_2} = 1 - \left(RH \cdot \frac{P_{sat}(T)}{P_{anode}}\right)$	$\left.\left(D_{O_2}^{eff}\frac{\partial C_{O_2}}{\partial x}\right)\right\vert_{x-\delta} = \left.\left(D_{O_2}^{eff}\frac{\partial C_{O_2}}{\partial x}\right)\right\vert_{x+\delta}$	$\left.\frac{\partial C_{O_2}}{\partial x}\right\vert_x = 0$	$C_{O_2} = 0, \frac{\partial C_{O_2}}{\partial x} = 0$	$C_{O_2} = 0, \frac{\partial C_{O_2}}{\partial x} = 0$	$C_{O_2} = 0, \frac{\partial C_{O_2}}{\partial x} = 0$
C_{H_2}	$C_{H_2} = 0, \frac{\partial C_{H_2}}{\partial x} = 0$	$C_{H_2} = 0, \frac{\partial C_{H_2}}{\partial x} = 0$	$C_{H_2} = 0, \frac{\partial C_{H_2}}{\partial x} = 0$	$\left.\frac{\partial C_{H_2}}{\partial x}\right\vert_x = 0$	$\left.\left(D_{H_2}^{eff}\frac{\partial C_{H_2}}{\partial x}\right)\right\vert_{x-\delta} = \left.\left(D_{H_2}^{eff}\frac{\partial C_{H_2}}{\partial x}\right)\right\vert_{x+\delta}$	$\chi_{H_2} = 1 - \left(C_{H_2O} \cdot \frac{RT}{P_{cathode}}\right)$
C_{H_2O}	$C_{H_2O} = RH \cdot \frac{P_{sat}(T)}{RT}$	$\left.\left(D_{H_2O}^{eff}\frac{\partial C_{H_2O}}{\partial x}\right)\right\vert_{x-\delta} = \left.\left(D_{H_2O}^{eff}\frac{\partial C_{H_2O}}{\partial x}\right)\right\vert_{x+\delta}$	$\left.\left(D_{H_2O}^{eff}\frac{\partial C_{H_2O}}{\partial x}\right)\right\vert_{x-\delta} = \left.\left(D_{H_2O}^{eff}\frac{\partial C_{H_2O}}{\partial x}\right)\right\vert_{x+\delta}$	$\left.\left(D_{H_2O}^{eff}\frac{\partial C_{H_2O}}{\partial x}\right)\right\vert_{x-\delta} = \left.\left(D_{H_2O}^{eff}\frac{\partial C_{H_2O}}{\partial x}\right)\right\vert_{x+\delta}$	$\left.\left(D_{H_2O}^{eff}\frac{\partial C_{H_2O}}{\partial x}\right)\right\vert_{x-\delta} = \left.\left(D_{H_2O}^{eff}\frac{\partial C_{H_2O}}{\partial x}\right)\right\vert_{x+\delta}$	$D_{H_2O}^{eff}\left.\frac{\partial C_{H_2O}}{\partial x}\right\vert_x = -\eta_d\frac{I}{F}$

Table S2. Parameters used in the PEMWE framework.

Parameter	**Unit**	**Value**	**Description**	**Reference**
Anode Porous Transport Layer (APTL)				
L_{APTL}	μm	200	thickness of APTL	[10]
ε_{APTL}	m^3/m^3	0.78	porosity of APTL	[11,12]
τ_{APTL}	m/m	1.132	tortuosity of APTL	
σ_{APTL}	S/m	2×10^4	electronic conductivity of Titanium	[10]
Anode Catalyst Layer (ACL)				
ρ_{ACL}	mg/cm^2	2	anode catalyst loading	
$\varepsilon_{i,ACL}$	wt. %	20	ionomer content	
L_{ACL}	μm	10	thickness of ACL	[10]
ε_{ACL}	m^3/m^3	0.551	porosity of ACL	[11,12]
τ_{ACL}	m/m	1.688	tortuosity of ACL	
σ_{ACL}	S/m	2×10^3	electronic conductivity of ACL ($Ir_xRu_{1-x}O_2$)	[10]
σ_{eff}	-	6.8×10^{-4}	effectiveness of electronic conductivity in porous ACL	
κ_{eff}	-	4.92×10^{-2}	effectiveness of ionomer conductivity in porous ACL	
a_{ACL}	m^2/m^3	15513043	electrochemical active interfacial area of ACL	
$r_{pore,ACL}$	nm	35	mean pore radius of anode catalyst layer	
Proton Exchange Membrane (PEM)				

L_{PEM}	μm	50	thickness of PEM	[10]
ε_{PEM}	m^3/m^3	0.35	porosity of PEM	
τ_{PEM}	m/m	1.69	tortuosity of PEM	
Cathode Catalyst Layer (CCL)				
ρ_{CCL}	mg/cm^2	0.3	cathode catalyst loading	
Pt/C	-	0.5	Pt/C ratio	
Ionomer/C	-	1	Ionomer/C ratio	
L_{CCL}	μm	10	thickness of CCL	[10]
ε_{CCL}	m^3/m^3	0.3275	porosity of CCL	[11,12]
τ_{CCL}	m/m	2.841	tortuosity of CCL	
σ_{CCL}	S/m	7.1428×10^4	electronic conductivity of CCL (Pt-C)	[10]
σ_{eff}	-	4.2×10^{-2}	effectiveness of electronic conductivity in porous CCL	
κ_{eff}	-	1.29×10^{-1}	effectiveness of ionomer conductivity in porous CCL	
a_{CCL}	m^2/m^3	22643378	electrochemical active interfacial area of CCL	
$r_{pore,CCL}$	nm	35	mean pore radius of CCL	
Cathode Porous Transport Layer (CPTL)				
L_{CPTL}	μm	200	thickness of CPTL	[10]
ε_{CPTL}	m^3/m^3	0.7	porosity of CPTL	[11,12]
τ_{CPTL}	m/m	1.195	tortuosity of CPTL	
σ_{CPTL}	S/m	1.25×10^3	electronic conductivity of carbon paper	[10]
Operating conditions				

T	K	343	operating temperature of water vapor	
P_{anode}	kPa	200	operating pressure at anode	[13]
$P_{cathode}$	kPa	200	operating pressure at cathode	
pH	-	0	pH of water vapor	
RH	%	100	relative humidity of water vapor	
n_d	-	0.2	electro-osmotic drag coefficient	[14]
V_{out}	mL/min	100	throughput of water and hydrogen mixture at the outlet	
Bubble dynamics (anode-centric)				
θ	deg	70	static contact angle of bubble on the electrode surface	
c_1	-	223.5	constant used for calculation of bubble distribution	
c_2	-	0.3204	constant used for calculation of bubble distribution	
n	-	2	total number of electrons transferred	
t_{res}	s	0.1	residence time for bubble detachment	
Charge-transfer reactions				
$i_{o,OER}$	A/cm^2	5×10^{-9}	exchange current density of OER	[15]
α_{OER}	-	2	charge transfer coefficient of OER	[11]
U^0_{OER}	V	1.23	OCP of OER at standard conditions	[11]
$i_{o,HER}$	A/cm^2	1×10^{-4}	exchange current density of HER	[15]
α_{HER}	-	0.7	charge transfer coefficient of HER	[12]
U^0_{HER}	V	0	OCP of HER at standard conditions	[12]

Table S3. Parameters used for validation of PEMWE framework.

Parameter	**Unit**	**Value**	**Description**	**Reference**
Anode Porous Transport Layer (APTL)				
L_{APTL}	μm	350	thickness of APTL	[10]
ε_{APTL}	m^3/m^3	0.78	porosity of APTL	[11,12]
τ_{APTL}	m/m	1.132	tortuosity of APTL	
σ_{APTL}	S/m	2×10^4	electronic conductivity of Titanium	[10]
Anode Catalyst Layer (ACL)				
L_{ACL}	μm	10	thickness of ACL	[10]
ε_{ACL}	m^3/m^3	0.2	porosity of ACL	[11,12]
τ_{ACL}	m/m	7.101	tortuosity of ACL	
σ_{ACL}	S/m	2×10^3	electronic conductivity of ACL ($Ir_xRu_{1-x}O_2$)	[10]
σ_{eff}	-	6.78×10^{-4}	effectiveness of electronic conductivity in porous ACL	
κ_{eff}	-	3.58×10^{-1}	effectiveness of ionomer conductivity in porous ACL	
a_{ACL}	m^2/m^3	15528674	electrochemical active interfacial area of ACL	
$r_{pore,ACL}$	nm	35	mean pore radius of anode catalyst layer	
Proton Exchange Membrane (PEM)				
L_{PEM}	μm	125	thickness of PEM	[10]
ε_{PEM}	m^3/m^3	0.35	porosity of PEM	

τ_{PEM}	m/m	1.69	tortuosity of PEM	
λ	-	31	Degree of humidification	[10]
Cathode Catalyst Layer (CCL)				
L_{CCL}	μm	10	thickness of CCL	[10]
ε_{CCL}	m^3/m^3	0.2	porosity of CCL	[11,12]
τ_{CCL}	m/m	5.248	tortuosity of CCL	
σ_{CCL}	S/m	7.1428×10^4	electronic conductivity of CCL (Pt-C)	[10]
σ_{eff}	-	1.67×10^{-2}	effectiveness of electronic conductivity in porous CCL	
κ_{eff}	-	2.65×10^{-1}	effectiveness of ionomer conductivity in porous CCL	
a_{CCL}	m^2/m^3	23274712	electrochemical active interfacial area of CCL	
$r_{pore,CCL}$	nm	35	mean pore radius of CCL	
Cathode Porous Transport Layer (CPTL)				
L_{CPTL}	μm	275	thickness of CPTL	[10]
ε_{CPTL}	m^3/m^3	0.7	porosity of CPTL	[11,12]
τ_{CPTL}	m/m	1.195	tortuosity of CPTL	
σ_{CPTL}	S/m	1.25×10^3	electronic conductivity of carbon paper	[10]

Table S4. Modeling parameters used in the PEMWE framework.

Parameters	**Unit**	**Value**
$\kappa_{ionomer,bulk}$	S/m	$100 \cdot e^{1268\left(\frac{1}{303}-\frac{1}{T}\right)} \cdot (0.005139\lambda - 0.00326)$
U_{OCP}	V	$1.229 - (0.9 \text{ x } 10^{-3}(T - 298))$
Ea_{anode}	kJ/mol	$11 + pH$
A_{anode}	mA $/cm^2$	$9.4 \text{ x } 10^{-7}$
$Ea_{cathode}$	kJ/mol	$85 + pH$
$A_{cathode}$	mA $/cm^2$	$620 \text{ x } 10^{-4}$
P_{sat}	Pa	$101325 \cdot 10^{-2.1794+(0.02953 \cdot T_S)-\left(9.1837 \text{ x } 10^{-5} \cdot T_S^2\right)+(1.4454 \text{ x } 10^{-7} \cdot T_S^3)}$ $T_s = T - 273.15$
D_{O_2}	m^2/s	$3.2 \text{ x } 10^{-5} \cdot \left(\frac{T}{353}\right)^{\frac{3}{2}} \left(\frac{P_0}{P}\right)$
D_{H_2}	m^2/s	$1.1 \text{ x } 10^{-4} \cdot \left(\frac{T}{353}\right)^{\frac{3}{2}} \left(\frac{P_0}{P}\right)$
D_{H_2O}	m^2/s	$7.35 \text{ x } 10^{-5} \cdot \left(\frac{T}{353}\right)^{\frac{3}{2}} \left(\frac{P_0}{P}\right)$

S6. Additional modeling results

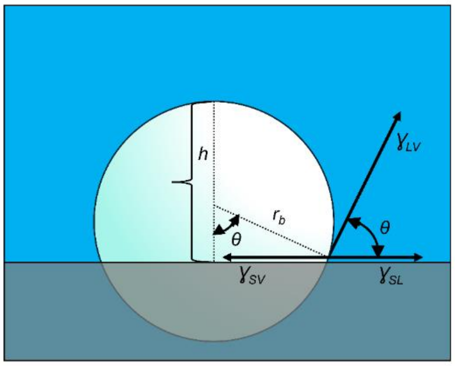

Fig S1. Schematic of a bubble just before detachment from a gas evolving electrode.

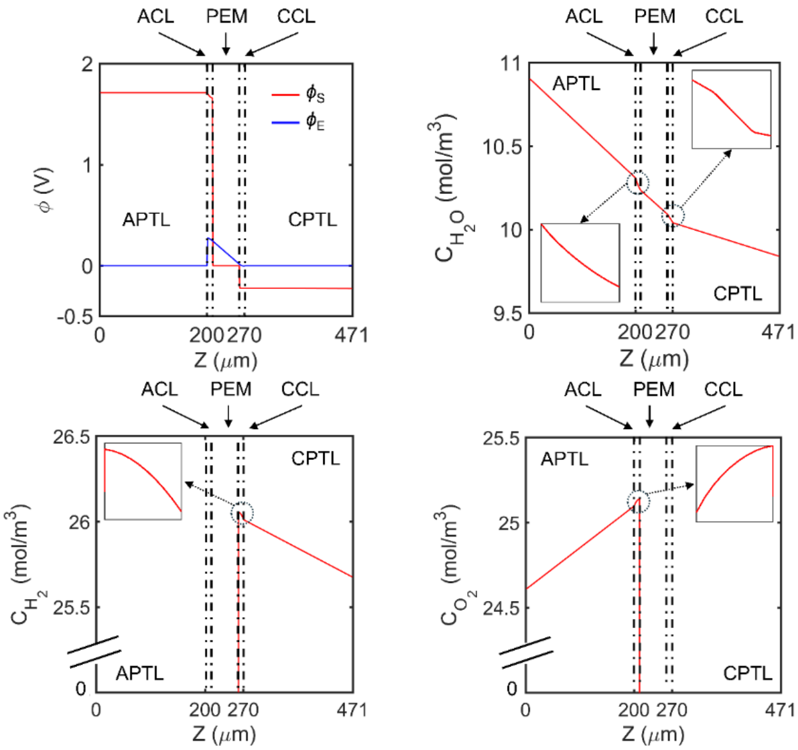

Fig S2. Variation of (a) solid and electrolyte potentials and concentrations of (b) H_2O, (c) H_2 and (d) O_2 inside the cell sandwich of a PEMWE operated with a current density of 1 A/cm^2 and a feed water temperature of 70^{o}C. The microstructural attributes, operating conditions and configuration of the PEMWE are summarized in Table S2.

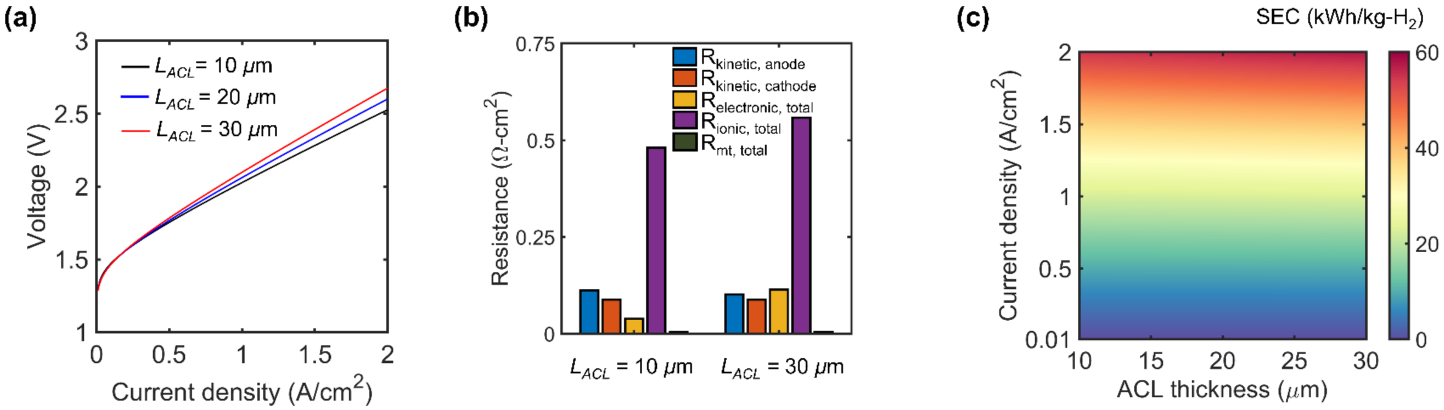

Fig S3. Impact of anode catalyst layer thickness on the (a) polarization, (b) resistance developed in a PEMWE cell sandwich at a current density of 2 A/cm^2. Other conditions pertaining to these results are summarized in Table S2. Coupled interplay of current density and catalyst layer thickness on the overall specific energy consumption of the PEMWE.

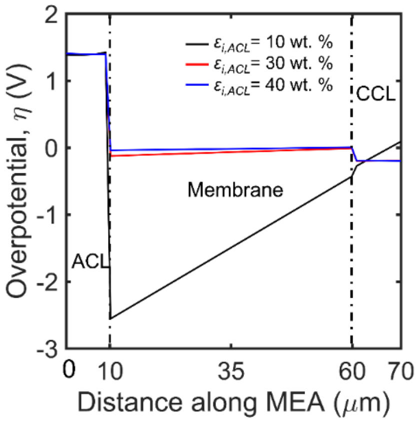

Fig S4. Spatial evolution of accrued overpotential along the membrane electrode assembly (MEA) under various ionomer content of the anode with a 0.5 mg/cm^2 catalyst loading, operated under a current density of 1 A/cm^2 and a feed water temperature of 70°C. Other configurational specifications of the PEMWE are summarized in Table S2.

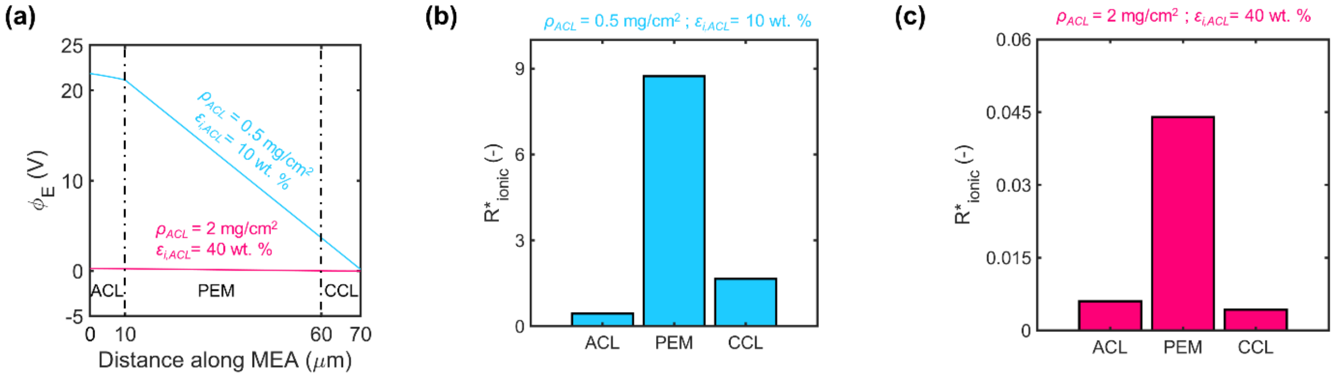

Fig S5. Impact of anode catalyst layer design on the (a) electrolyte potential, dimensionless ionic resistance developed in the MEA at an anode recipe of (b) 0.5 mg/cm^2; 10 wt.% ionomer and (c) 2 mg/cm^2; 40 wt.% ionomer operated at a current density of 2 A/cm^2 and 70^{o}C feed water temperature.

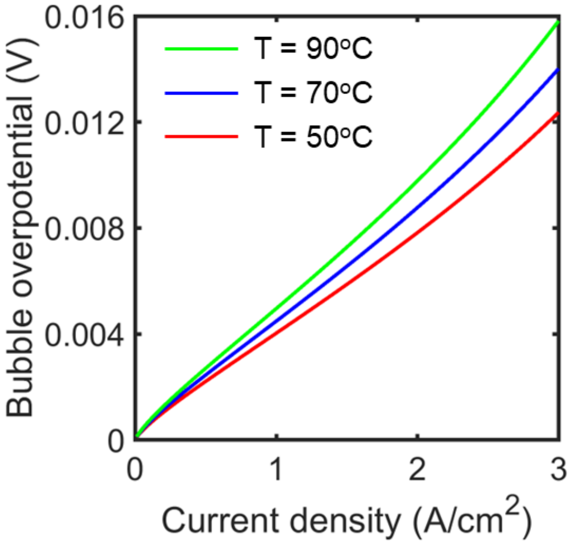

Fig S6. Impact of feed water temperature on the bubble overpotential response at RH = 100%. Other configurational specifications of the PEMWE are summarized in Table S2.

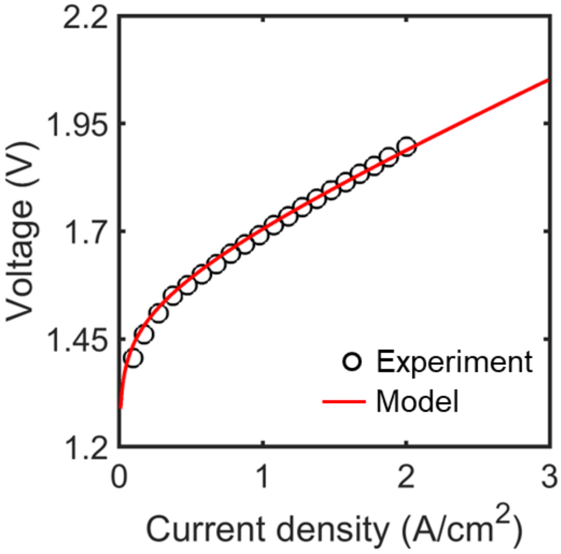

Fig S7. Polarization response of our validated PEMWE framework against experimental data from Han et. al[10] at higher current densities (up to 3 A/cm^2). The modeling parameters are specified in Table S3.

References

1 L. C. Weng, A. T. Bell and A. Z. Weber, *Physical Chemistry Chemical Physics*, 2018, **20**, 16973–16984.

2 L. C. Weng, A. T. Bell and A. Z. Weber, *Energy Environ Sci*, 2019, **12**, 1950–1968.

3 X. Su, L. Xu and B. Hu, *Int J Hydrogen Energy*, 2022, **47**, 20027–20039.

4 Y. Li, Z. Kang, J. Mo, G. Yang, S. Yu, D. A. Talley, B. Han and F. Y. Zhang, *Int J Hydrogen Energy*, 2018, **43**, 11223–11233.

5 R. Iwata, L. Zhang, K. L. Wilke, S. Gong, M. He, B. M. Gallant and E. N. Wang, *Joule*, 2021, **5**, 887–900.

6 N. Goswami, A. N. Mistry, J. B. Grunewald, T. F. Fuller and P. P. Mukherjee, *J Electrochem Soc*, 2020, **167**, 084519.

7 N. Goswami, J. B. Grunewald, T. F. Fuller and P. P. Mukherjee, *J Mater Chem A Mater*, 2022, **10**, 15101–15115.

8 GeoDict simulation software Release 2024, by Math2Market GmbH, Germany, https://www.math2market.com/geodict-software/geodict-software-download.html, (accessed 20 August 2024).

9 A. N. Mistry, K. Smith and P. P. Mukherjee, *ACS Appl Mater Interfaces*, 2018, **10**, 6317–6326.

10 B. Han, J. Mo, Z. Kang and F. Y. Zhang, *Electrochim Acta*, 2016, **188**, 317–326.

11 L. C. Weng, A. T. Bell and A. Z. Weber, *Energy Environ Sci*, 2019, **12**, 1950–1968.

12 L. C. Weng, A. T. Bell and A. Z. Weber, *Physical Chemistry Chemical Physics*, 2018, **20**, 16973–16984.

13 B. Han, S. M. Steen, J. Mo and F. Y. Zhang, *Int J Hydrogen Energy*, 2015, **40**, 7006–7016.

14 F. Marangio, M. Santarelli and M. Calì, *Int J Hydrogen Energy*, 2009, **34**, 1143–1158.

15 D. S. Falcão and A. M. F. R. Pinto, *J. Clean. Prod.*, 2020, **261**, 121184.